

---

# Imaging Techniques

Robert Hermans, Frederik De Keyzer, Vincent Vandecaveye,  
and Laurens Carp

## Contents

<b>1</b>	<b>Introduction</b> .....	33
<b>2</b>	<b>Plain Radiography</b> .....	34
<b>3</b>	<b>Ultrasonography</b> .....	34
<b>4</b>	<b>Computed Tomography and Magnetic Resonance Imaging</b> .....	34
4.1	Computed Tomography .....	36
4.2	Magnetic Resonance Imaging .....	39
<b>5</b>	<b>Nuclear Imaging</b> .....	49
5.1	Physical Aspects .....	49
5.2	Radiopharmaceuticals .....	50
5.3	Technical Aspects of FDG-PET and Integrated FDG-PET/CT in Head and Neck Cancer .....	51
	<b>References</b> .....	53

---

## Abstract

Various imaging techniques are used to investigate the presence and extent of head and neck neoplasms, including ultrasound, computed tomography, magnetic resonance imaging and nuclear imaging techniques. To obtain the most optimal results, close attention should be paid to a correct technical execution of the imaging study. This chapter provides information on the relative advantages and disadvantages of each of the available imaging techniques, as well as on patient preparation, contrast agent or tracer injection, data acquisition, and image reconstruction, reformatting and display. The possible value of some newer imaging techniques, such as diffusion-weighted MRI and dynamic contrast-enhanced MRI is also reviewed.

---

## 1 Introduction

Various imaging techniques are used in the evaluation of patients with head and neck cancer, before, during and after treatment. Each of these imaging techniques has its own advantages and disadvantages.

Many head and neck neoplasms arise from the mucosal lining; when a patient is referred for imaging, the histological diagnosis often was already established by endoscopic biopsy. Therefore, imaging should primarily supply information on the submucosal extension depth of the primary tumor, including its relation to surrounding structures, as well as on the presence of regional and/or distant metastasis, or a second primary tumor.

---

R. Hermans (✉) · F. De Keyzer · V. Vandecaveye  
Department of Radiology, University Hospitals Leuven,  
Herestraat 49, 3000 Leuven, Belgium  
e-mail: robert.hermans@uzleuven.be

L. Carp  
Service of Nuclear Medicine,  
University Hospital Antwerp, Wilrijkstraat 10,  
2650 Edegem, Belgium

The purpose of this chapter is to describe the various techniques available for imaging the head and neck cancer patient, and to provide general rules for their use. Specialized imaging applications are described in the following chapters where appropriate.

---

## 2 Plain Radiography

In the past, a variety of conventional methods were applied to stage head and neck cancer, including soft tissue views of the neck, plain films of the facial skeleton, xeroradiography, plain film tomography, laryngography and barium swallow. The value of these studies to stage head and neck cancer is very limited; these techniques are now replaced by cross-sectioning imaging modalities.

Barium swallow remains an indispensable method in the early phase after pharyngeal surgery, to rule out or confirm the presence of fistulae. This technique is also essential in the evaluation of functional disorders (such as bolus retention, delayed passage and aspiration) after surgery or radiotherapy.

---

## 3 Ultrasonography

Ultrasonography is a widely used technique for the evaluation of the thyroid gland (see “[Thyroid and Parathyroid Neoplasms](#)”), neck lymph nodes (see “[Neck Nodal Disease](#)”) and salivary glands, as it offers visualization of these structures with high spatial resolution, at a low cost and without using ionizing radiation.

Ultrasonography in combination with fine needle aspiration cytology (FNAC) is the most accurate method for neck nodal staging in most head and neck cancers (Van Den Brekel et al. 1991). However, execution of this procedure is time consuming, and the obtained results are operator-dependent (Takes et al. 1996). Also, in a multicenter study where both computed tomography and ultrasound of the neck were applied for staging of head and neck cancer, the addition of ultrasound-guided FNAC did not provide significant additional value (Takes et al. 1998).

---

## 4 Computed Tomography and Magnetic Resonance Imaging

Nowadays, in most patients computed tomography (CT) or magnetic resonance imaging (MRI) is performed for pretherapeutic staging of a head and neck malignancy. Both techniques can supply the information needed by the clinician for adequate treatment planning.

A common question is which of these techniques should be used in a particular patient. The most widely used technique is CT, as it has a number of important advantages over MRI:

- wide availability
- relative low cost
- easy to execute this in a reproducible way
- short examination time, resulting in less image quality degradation caused by motion, such as swallowing and respiration
- superior bone detail
- high quality multiplanar imaging on multidetector CT systems
- easy extend of the study into the upper thoracic cavity or intracranial cavity, if needed
- easier interpretation, especially regarding nodal involvement (Curtin et al. 1998).

However, CT also has a number of disadvantages compared to MRI:

- relative low soft tissue contrast resolution
- administration of iodinated contrast agent is necessary
- severe image quality degradation by dental fillings or other metallic foreign objects (Fig. 1)
- radiation exposure.

The advantages of MRI over CT in the evaluation of head and neck cancer are its superior soft tissue contrast resolution, and the absence of radiation exposure. Overall, the image quality is not or less hampered by the presence of dental fillings than in CT, but also MRI studies may be severely jeopardized by metallic implants (Fig. 2). The disadvantages of MRI are mainly related to the long acquisition time, making the technique sensible to motion artifacts which cause a non-diagnostic study (Fig. 3). It is also technically more challenging with MRI to properly

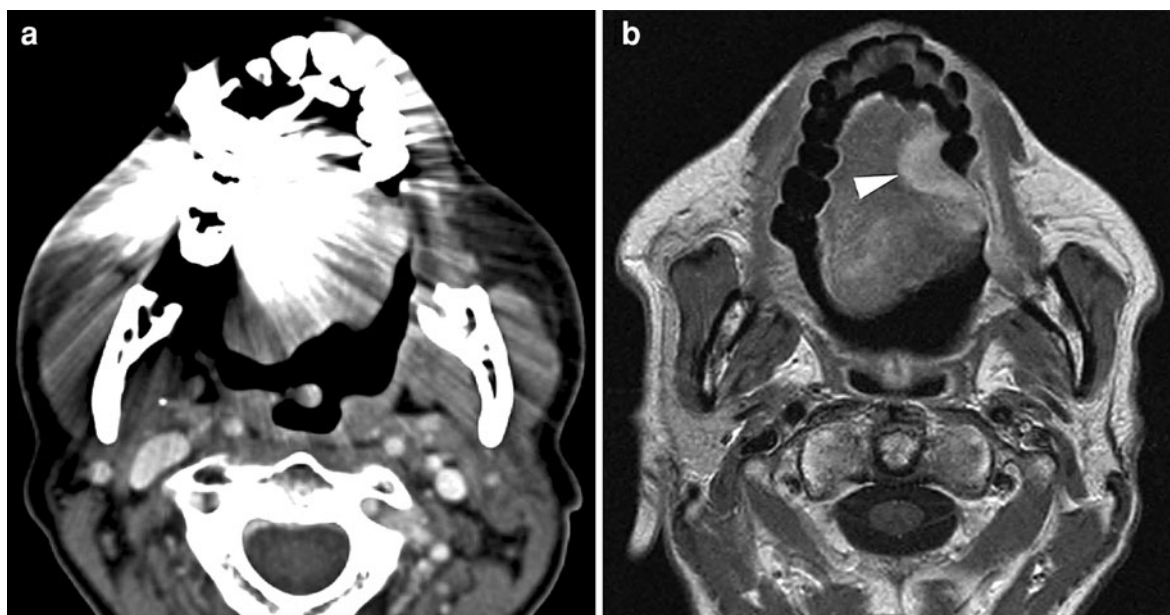


**Fig. 1** Patient suffering left-sided oral tongue cancer. **a** Axial contrast-enhanced CT-image. As the image quality is severely hampered by artifacts arising from dental fillings, the primary tumor is not visible. A complementary MR-study was advised.

**b** Gadolinium-enhanced T1-weighted image, not affected by presence of dental fillings, clearly shows the primary tumor (*arrowhead*)

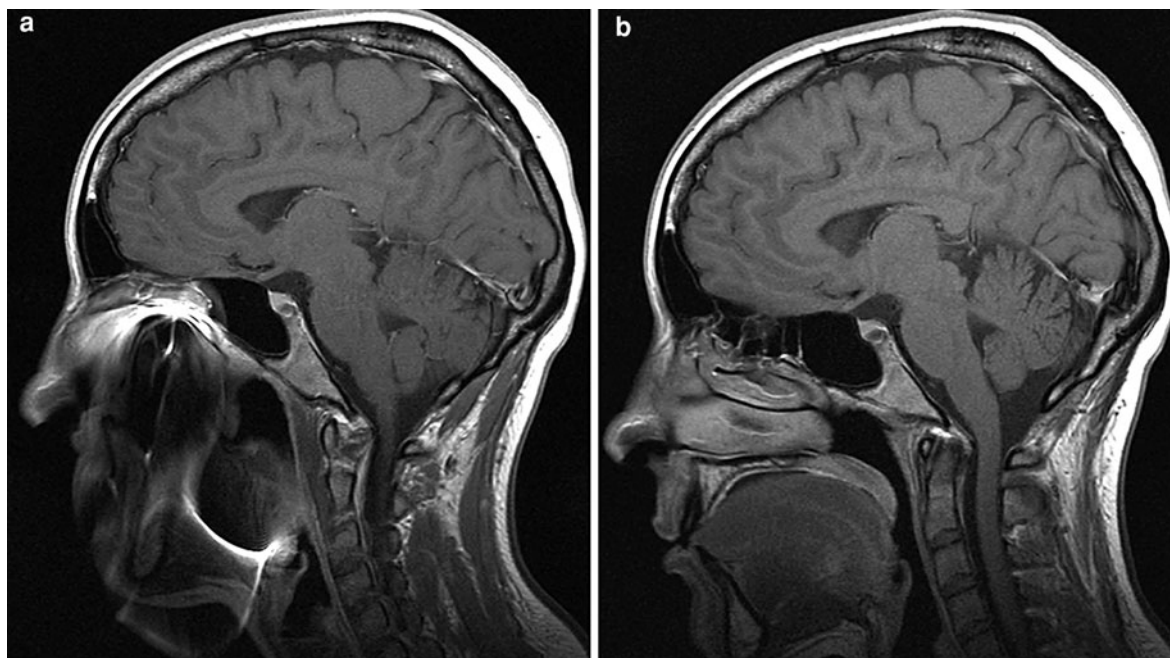


**Fig. 2** Patient referred for MR-study of the maxillofacial region and skull base because of unilateral facial pain. **a** Initial MR-study was non-conclusive, as artifacts caused by fixed

orthodontic material severely degrade image quality. **b** After removal of the orthodontic material by the dentist, optimal image quality was achieved

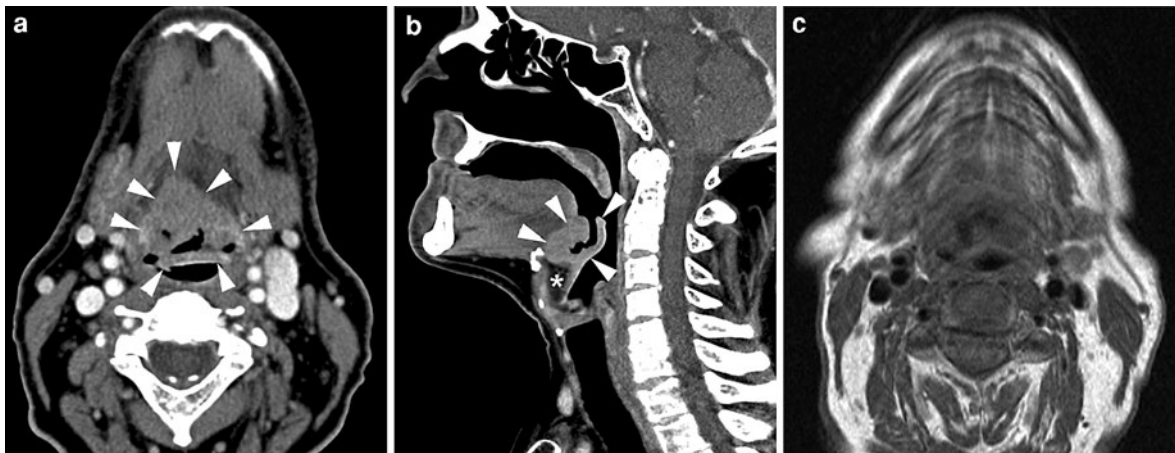


**Fig. 3** Patient suffering tongue base cancer. **a, b** Axial and sagittal reformatted contrast-enhanced MDCT-images clearly show tumor extent into tongue base and involvement of free epiglottic rim (*arrowheads*), as well as the relationship of the

tumor to the pre-epiglottic space (*asterisk*). **c** For study purposes, a MR-study was performed in this patient one day later. Because of motion artifacts, the tumor is not confidently discernable. This MR-study was considered non-diagnostic

stage both primary tumor and neck nodal disease in a single study. The lower availability of MRI, resulting in a longer waiting list, and its higher cost should also be taken into consideration.

In many institutions, CT is the preferred imaging method for evaluation of laryngeal and hypopharyngeal cancer, as well as of oral cavity and oropharyngeal cancer. These cancer sites constitute about 80–85% of all head and neck malignancies (excluding skin cancer and lymphoma) in Europe and the USA. In most cases, a dedicated CT study will provide all answers needed by the clinician; in such a setting, MRI is used as complementary tool to solve remaining questions.

Because of its higher contrast resolution, MRI is the preferred imaging method in rarer head and neck malignancies, such as nasopharyngeal cancer and sinonasal cancer. There is no consensus regarding the use of CT or MRI as primary imaging tool in salivary gland cancer, although there is a tendency among head and neck radiologists to choose for MRI.

## 4.1 Computed Tomography

CT can be regarded as the ‘workhorse’ of head and neck cancer imaging. It is not possible to define the ideal imaging protocol, as available equipment varies. The minimal requirements for an optimal diagnostic study will be outlined.

### 4.1.1 Patient Positioning

The images are obtained with the patient supine and during quiet respiration. The neck should be in slight extension. The head is aligned in the cephalocaudal axis in order to make it possible to compare symmetric structures. Malposition may result in an appearance that simulates disease. Every effort should be made to make the patient feel comfortable; this will help the patient dropping the shoulders to a position as low as possible (Wirth et al. 2006).

This patient-friendly position is applicable for all indications if multidetector spiral CT (MDCT) is used, as this modality allows retrospective high quality reformatting in every spatial plane. In case an incremental or single-spiral CT technique has to be used, additional direct coronal imaging is needed in the evaluation of sinonasal and skull base neoplasms. This can be realized by hyperextension of the neck, either in supine or prone position, and tilting the gantry to a position perpendicular to the hard palate.

### 4.1.2 Contrast-Agent Injection

While evaluating a patient suffering head and neck cancer, a proper injection method of iodinated contrast agent is crucial to obtain state-of-the art CT-images. Optimal tissue enhancement, allowing correct discrimination of tumoral from normal tissue, and a high neck vessel density must be realized at the same time. Several contrast-agent injection protocols have been described, some of them being fairly

complicated. For all practical purposes, a single bolus technique with an injection rate of 1–2 cc/s is appropriate on modern CT machines (Keberle et al. 2002). A total amount of 100 ml is sufficient in MDCT; a somewhat higher volume (up to 150 ml) may be required when an incremental or single-slice spiral CT technique is used.

It is essential to wait long enough before starting the acquisition, as the contrast agents need some time to diffuse in the normal and pathologic soft tissues. If re-angulation of the gantry at the oral level is performed (see below), the contrast injection needs not to be paused while changing the gantry angle. If one uses an MDCT-machine, allowing a rapid entire neck examination without gantry angulation, the scan should be started only after injection of the entire contrast volume. A subsequent saline injection at the same injection rate is recommended. The contrast-agent injection protocol for evaluation of the head and neck, as currently used in Leuven is: 1.5 cc/s contrast agent up to 100 ml, followed by 30 ml saline at the same rate; image acquisition starts 80 s after initiation of the injection.

### 4.1.3 Data Acquisition and Image Reconstruction

#### 4.1.3.1 General Comments

On a lateral scout view, the area of interest is indicated. For a routine head and neck imaging study, images are acquired from the top of the sphenoid sinus to the lower border of the sternoclavicular joints. It makes sense to scan from cranial to caudal: this allows the contrast medium concentration in the subclavian vein, at the side of injection, to drop to a similar or only slightly higher level compared to other neck vessels, reducing artifacts at the level of the thoracic inlet.

When performing a routine study of the face, sinusal region or skull base, images are acquired from the top of the frontal sinus to the submental region.

The field of view (FOV) must be as small as possible, to optimize spatial resolution. The recommended FOV for neck studies varies between 16 and 20 cm, depending on the size of the patient. The selected FOV also depends on the type of pathology: in a study performed for squamous cell cancer, the posterior part of the perivertebral space not necessarily needs to be included in the FOV as it is unlikely to encounter pathology in that region;

however, for example in skin cancer and lymphoma, this part of the neck should also be visualized, as (sub) occipital adenopathies may be present.

The optimal display slice thickness for evaluation of neck structures is 3 mm; adjacent slices should be obtained. Somewhat thinner slices (2 mm) are apt for the evaluation of the facial bones, sinonasal cavities and orbits. In laryngeal and hypopharyngeal neoplasms, it is useful to reconstruct an additional series of images coned down to the laryngohypopharyngeal region, with a FOV of about 10 cm and a slice thickness of 2 mm. Also the evaluation of the temporal bone requires a coned down FOV (about 9 cm), and a thin slice thickness of 0.5–1 mm.

Image reconstruction is always done in a soft tissue algorithm. Additional images, reconstructed in a high-resolution (bone detail) algorithm, are always generated in sinonasal cavity, skull base and temporal bone studies.

In patients suffering neoplastic disease, the lower slices including the upper part of the lungs should also be reviewed in lung window, as unknown metastatic disease or second primary tumors may then become visible.

#### 4.1.3.2 Incremental CT and Single-Slice Spiral CT

Even in this era of MDCT, studies of acceptable quality can be obtained using an incremental or single-slice spiral CT technique. The disadvantage of these techniques is the compromise that has to be made between slice thickness and acquisition time. As these techniques do not allow obtaining very high quality reformattings from the native images, the gantry angle should be changed at the mouth level. From the skull base down to the oral cavity, the image plane should be parallel to the hard palate, while from the oral cavity down to the thoracic inlet, the image plane should be parallel to the vocal cords. The vocal cord plane sometimes can be recognized on the lateral scout views; if this cannot be seen, the gantry should be tilted parallel to the intervertebral disk space at the level of C4–C5 or C5–C6. Adherence to this protocol generates images reproducibly showing head and neck anatomy; furthermore, dental filling artifacts are avoided at the level of the oral cavity.

The CT examination is performed as contiguous 3 mm thick scans, or as a spiral study reconstructed as contiguous 3 mm sections. The spiral technique uses 3 mm thick scans with a 3–5 mm/s table speed, and a

pitch of 1:1–1:1.6; these parameters may vary slightly according to the CT machine.

#### 4.1.3.3 Multidetector Spiral CT

State-of-the-art CT of the head and neck requires the use of MDCT. The rapid acquisition results in a volumetric data set, reconstructed to a stack of thin and overlapping native images; this reduces partial volume averaging and motion artifacts. Furthermore, full advantage of the injected contrast agent is accomplished by optimal timing between injection and image acquisition. Disadvantage of this technique is the overall higher radiation exposure.

The native images cannot routinely be used for display: the large amount of native images is difficult to handle, and the signal/noise level of these images is relatively low. Therefore, a new set of images needs to be reformatted from these native images for display. These images are routinely reformatted in the axial plane, mimicking the image display as it is obtained in incremental or single-slice spiral CT: for neck studies, adjacent 3 mm thick images are reformatted parallel to the hard palate from the skull base to the oral cavity, and parallel to the vocal cords from the oral cavity to the thoracic inlet (Fig. 4). Reformating in other planes and/or with a thinner slice thickness is done according to the organ of interest (see above) and/or the findings on the axial images (Fig. 5).

The data acquisition with MDCT is usually done with zero gantry tilt. However, in some patients, this causes problems at the level of the oral cavity when dental fillings are present. Also, in patients with short necks or a high position of the shoulders, the image quality may be suboptimal at the level of the larynx due to artifacts arising from the shoulder girdle. To avoid these problems, some head and neck radiologists continue to use gantry tilting in MDCT, as described for the incremental and single-slice spiral CT technique, although this makes it impossible to obtain reformatted images in the coronal or sagittal plane at the level of the oral cavity. An alternative is to perform a complete head and neck study without gantry tilt, and acquire additional images the level of the oral cavity and oropharynx, if dental filling artefacts are present, with a tilted gantry (Fig. 6). Yet another solution is to obtain additional images with the mouth widely opened; this may bring the pathology out of the dental filling artifacts (Fig. 7) (Henrot et al. 2003).

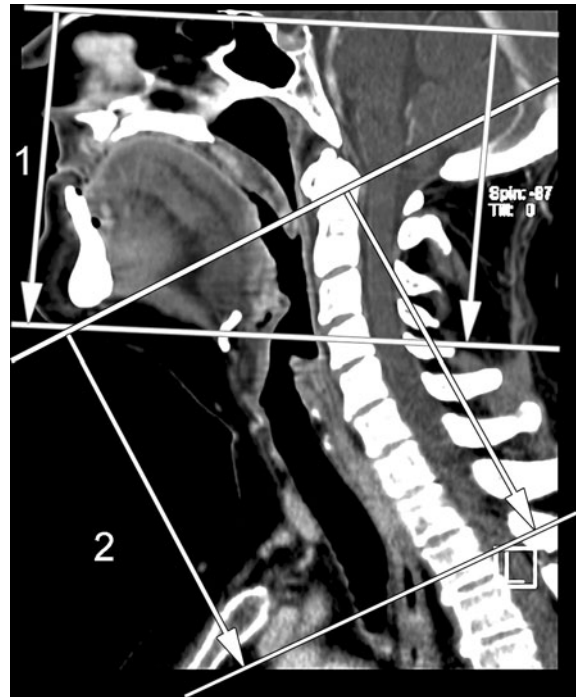


**Fig. 4** Routine head and neck CT-study. Midline sagittally reformatted image from native axial MDCT-images. The data acquisition extended from just above the sphenoid sinus to the thoracic inlet. From the native images, two sets of axial images are routinely reformatted for display: the first set (1), parallel to the hard palate, from the skull base to the lower margin of the mandible; the second set (2), parallel to the vocal cords (or C4–C5/C5–C6 intervertebral space), from the oral cavity to the thoracic cavity. The two image sets should be overlapping

More technical details on the MDCT-parameters used currently in the University Hospitals of Leuven are summarized in Table 1 and 2.

#### 4.1.4 Dynamic Maneuvers

The data acquisition is routinely performed while the patient continues breathing. Dynamic maneuvers during scanning can improve the visualization of particular anatomic structures. During prolonged phonation of [i], arytenoid mobility can be judged and a better visualization of the laryngeal ventricle can be achieved; the slight distention of the pyriform sinuses may also allow better delineation of the aryepiglottic folds (Lell et al. 2004). A modified Valsalva maneuver (blowing air against closed lips, puffing out the cheeks) produces substantial dilatation of the hypopharynx, allowing better visualization of the pyriform sinuses, including the postericoid region (Robert et al. 1993) (Fig. 8).



**Fig. 5** **a** Axial MDCT-image (3 mm thick) shows lymph node on right side, appearing centrally hypodense (*arrowhead*): central necrosis or partial volume averaging of fatty nodal hilum? **b** Additionally, a thinner (1.5 mm) reformatting was

made through this lymph node in the coronal plane. On this section, the hypodense nodal region shows fat density and communicates with the outer nodal border: fatty metaplasia in nodal hilum. Normal lymph node

This modified Valsalva maneuver may also be of use in the evaluation of oral cavity tumors, as the inner cheek walls and gingivobuccal sulci become better visible.

The success rate of these dynamic maneuvers is variable, especially when an incremental CT technique is used, and is strongly depending on the cooperation of the patient. These problems are largely overcome by MDCT, as the patient has to perform the maneuver only once during one rapid acquisition.

Dynamic maneuvers are mainly helpful in showing superficial tumor spread, while the purpose of imaging is describing deep tumor extent. Also, abnormal mobility of the vocal cord is more accurately seen during clinical examination than on dynamic imaging studies. Therefore, the added value of acquiring images during a dynamic maneuver in staging head and neck neoplasms is, on average, limited.

#### 4.1.5 Three-Dimensional Image Reformatting

Three-dimensional (3D) display of the data set is most often done to evaluate the bony structures of the maxillofacial skeleton in congenital abnormalities or traumatic lesions. Meaningful 3D display of the often subtle osteolytic changes seen in head and neck malignancies is rarely possible. However, in some cases of extensive

bone destruction, 3D displays are helpful for the surgeon in planning bone resection (Fig. 9).

Virtual endoscopy of the larynx and hypopharynx has been studied; otolaryngologists rank such 3D images as more beneficial than radiologists, usually in bulky masses that precluded definitive direct endoscopic evaluation (Silverman et al. 1995). This technique does not show the adjacent soft tissues, and its clinical role is not exactly defined (Magnano et al. 2005).

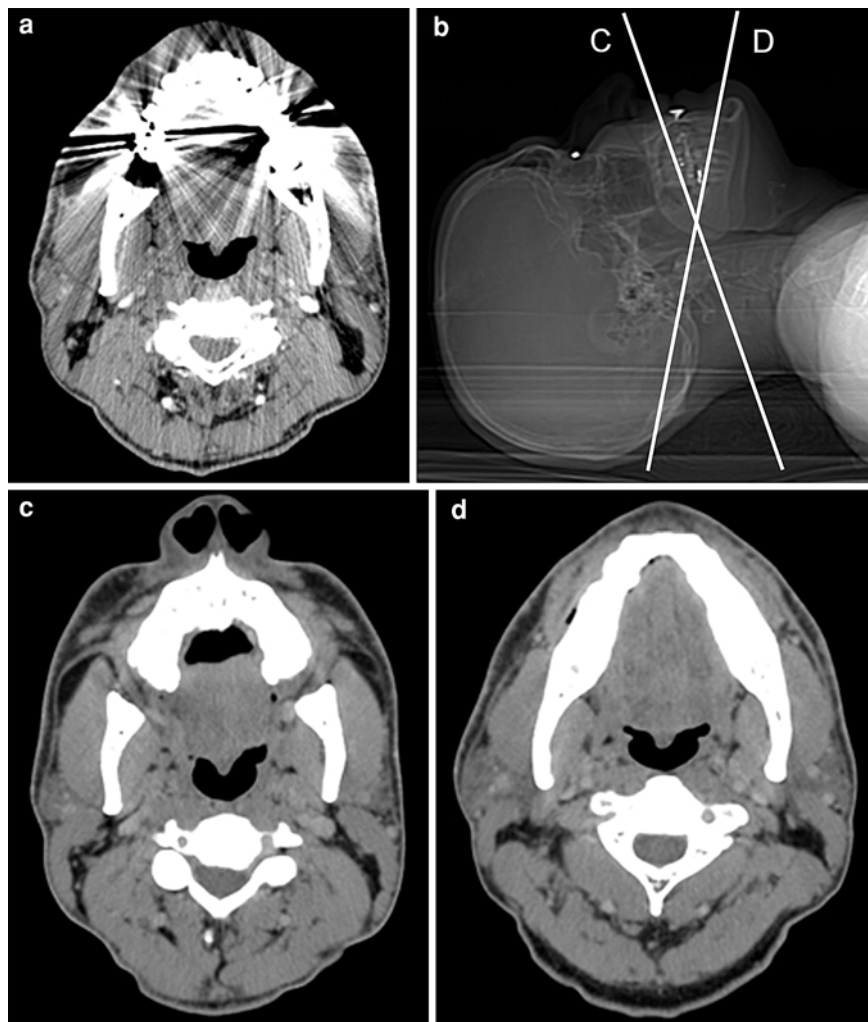
## 4.2 Magnetic Resonance Imaging

MRI of the head and neck can be performed on low-field or high-field machines. At comparable measuring time, the high-field ( $\geq 1.5\text{T}$ ) machines provide a better signal-to-noise ratio and a higher spatial resolution. Currently, the experience on 3T systems regarding the investigation of head and neck tumors is steadily increasing.

### 4.2.1 Patient Positioning

Similar to CT, the image acquisition is performed with the patient in supine position, and during quiet respiration. The head and neck should be aligned and symmetrically positioned. Every effort should be

**Fig. 6** Axial MDCT-image at level of oral cavity and oropharynx, obtained with a zero degree gantry tilt (a), is severely degraded by artifacts arising from dental fillings. By obtaining additional images with angulation of the gantry around the dental fillings (b), optimal image quality could be achieved at this level (c, d). (Courtesy of Ilona Schmalfluss, MD, Gainesville, FL, USA)



made to make the patient feel as comfortable as possible. The patient should be instructed not to move during the examination, and to try not to cough during the image acquisition. The patient should not be prohibited to swallow as this is hardly feasible in clinical practice as the imaging sequences take several minutes each.

#### 4.2.2 Coils

The choice of the receiver coil is dictated by the localization of the disease process. If the tumor is localized in the oral cavity or infrahyoid part of the neck, the neck coil should be used. When the patient suffers neoplastic disease at the level of the skull base, sinonasal cavities, face, parotid glands or nasopharynx, the head coil should be selected. A disadvantage of

using a single receive coil however is the inability to cover the entire neck for evaluation of nodal stations.

This may be of particular importance in nasopharyngeal, tongue or oropharyngeal cancer which are frequently associated with adenopathies throughout the neck. Modern machines, at field strengths of 1.5 and 3 T, allow to image the entire head and neck, either by a combination of a standard head coil and 2-channel dedicated surface coil or an integrated head-neck coil of 12 or more coil elements.

A possible drawback of combining head and neck coils is that both coils have a distinctive coil design, inducing heterogeneous recipient field characteristics at the crossover between the two coils, which translates into local signal loss, distortion and heterogeneous incomplete fat saturation. This drawback can be partially

**Fig. 7** Patient suffering cancer of the lateral tongue edge. **a, b** Sagittal and axial reformatted CT-image, obtained after a standard MDCT acquisition with closed mouth (**a**). This study did not show the extent of the primary tumor because of dental filling artifacts (**b**). Tilting the gantry would not have solved the problem in this patient, as the dental fillings are close to the tumor. **c, d** Because of a contra-indication for MRI, an additional CT-study was performed with the mouth of the patient widely opened (**c**). This brings the region of the tongue tumor (**d**, arrowheads) out of the dental filling artifacts



overcome by meticulous shimming, coil and patient position and the use of sequences with short echo-trains. As such, an integrated head-neck coil that provides a homogeneous pattern of full receiver coil coverage with a high signal-to-noise ratio and minimized artifacts is preferred for imaging of the entire head and neck.

#### 4.2.3 Standard Sequences

After obtaining scout images, a standard examination of the head and neck should start with a T2-weighted turbo spin-echo (TSE) sequence. Compared to a conventional T2-weighted spin-echo (SE) sequence, a TSE sequence takes less time to perform, reducing motion artifacts and improving image quality. However, the high signal intensity of fat on a T2-weighted TSE sequence can be a disadvantage, as this may reduce the contrast between a tumor and the surrounding tissues. The contrast can be improved by performing the sequence with either a

chemical shift-moderated fat suppression technique (chemical shift-selective fat suppression or water-selective excitation) or by applying an additional inversion recovery preparation pulse with a short inversion time (SPIR, SPAIR, STIR).

The high signal intensity of fat and bone marrow on a plain T1-weighted SE or TSE sequence is often very helpful to determine tumor extent, as it contrasts clearly with the low signal intensity of most tumors. Repetition of this sequence after injection of gadolinium-DTPA, and comparison with the pre-injection sequence, allows to determine the areas of contrast-enhancement and to differentiate these areas from fat.

A fat-saturated T1-weighted SE sequence after injection of gadolinium-DTPA may be helpful, as the contrast between enhancing tissue and fat is increased, but at the cost of some more susceptibility artifacts and a longer acquisition time.

**Table 1** MDCT data acquisition and native image reconstruction parameters

		16-row	64-row	128-row
Neck <sup>a</sup> Face <sup>b</sup> Sinonasal cavities <sup>b</sup>	Collimation	16 × 0.75 mm	64 × 0.6 mm	128 × 0.6 mm
	Feed/rotation	10.2	17.3 mm	30.7 mm
	Rotation time	1 s	1 s	1 s
	kV	120	120	120
	mAs <sub>eff</sub>	250 <sup>c</sup>	250 <sup>c</sup>	230 <sup>c</sup>
	slice <sub>eff</sub>	1 mm	1 mm	1 mm
	slice interval	0.7 mm	0.7 mm	0.5 mm
Temporal bone <sup>b</sup> Skull base <sup>b</sup>	Collimation	2 × 0.6 mm	12 × 0.3 mm	16 × 0.3 mm
	Feed/rotation	1.2 mm	1.8 mm	4 mm
	Rotation time	1 s	1 s	1 s
	kV	140	140	140
	mAs <sub>eff</sub>	220	260	240
	slice <sub>eff</sub>	0.6 mm	0.6 mm	0.4 mm
	slice interval	0.2 mm	0.2 mm	0.2 mm

mAs<sub>eff</sub> = effective mAs

slice<sub>eff</sub> = effective slice thickness

<sup>a</sup> soft tissue algorithm

<sup>b</sup> both soft tissue and bone detail algorithm in tumoral pathology

<sup>c</sup> effectively used mAs may be lower (determined by automatic exposure control system)

**Table 2** MDCT-image reformatting for display

	Slice thickness	Slice interval	Image plane
Neck	3 mm	3 mm	Axial + coronal + sagittal
Face, sinonasal cavities, skull base (soft tissue detail)	2 mm	2 mm	Axial + coronal + sagittal
Temporal bone, skull base (bone detail)	0.8 mm	1	Axial + coronal (sagittal if needed)

Depending on the investigated region, a slice thickness of 3–4 mm is optimal, with an interslice gap of 0–50%. The FOV is similar to what is described above for CT. The imaging matrix should be at least 256 × 256, but in recent years more often a base matrix of 384 or 512 is advocated, especially for lesions in and around the skull base and sinonasal cavities.

The plane of section is chosen according to the localization of the disease process. For most neck lesions, it is appropriate to start with a T2- and T1-weighted sequence in the axial plane, and to continue with a gadolinium-enhanced axial, coronal and sagittal T1-weighted sequence. In general, the axial plane should be, similar as for CT, parallel with the hard palate when dealing with suprahyoid pathology, and parallel with the vocal cords when dealing with infrahyoid pathology. In naso-ethmoidal neoplasms, it

may be more useful to start the study with a coronal T2- and T1-weighted sequence, in order to better evaluate potential spread to the anterior cranial fossa.

The use of very fast imaging such as single-shot techniques is usually not recommended. Single-shot techniques have in general a lower signal-to-noise ratio and are very sensitive to magnetic field inhomogeneities (susceptibility effects). Also, single-shot sequences often yield a somewhat blurred image, impairing visualization of thin structures or making accurate delineations. In case of uncooperative patients or when fast scan time is absolutely required, patient positioning and shimming should be performed with the utmost precision. If patient movement is within limits, a segmented approach, probing the entire k-space into several separate acquisitions and thereby reducing the echo-train length, is preferable to minimize the above-mentioned drawbacks.

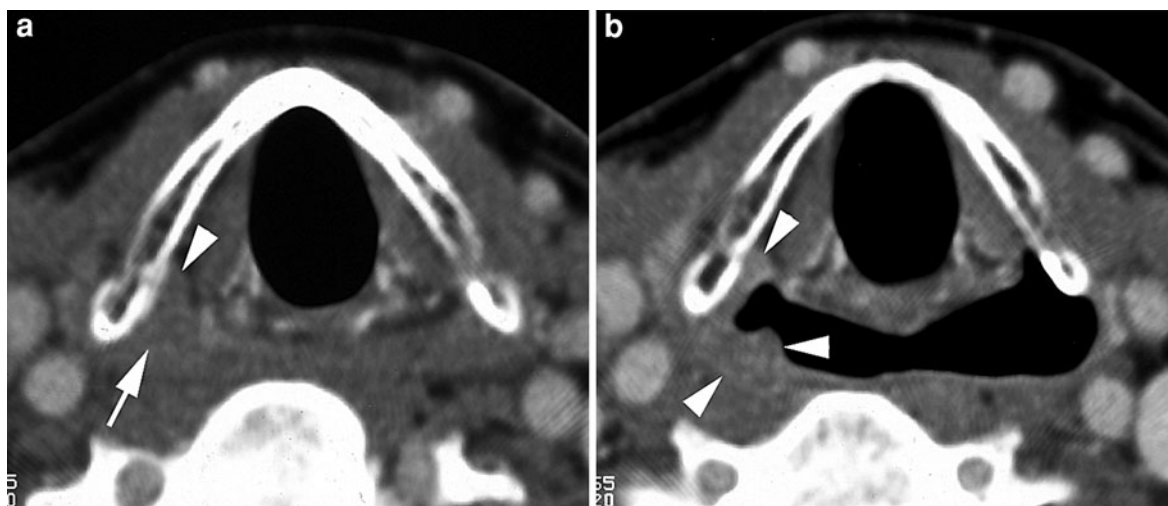


**Fig. 8** Contrast-enhanced single-slice spiral CT-images in a patient suffering cancer of the pyriform sinus. **a** Axial image during quiet breathing shows subtle soft tissue thickening in the apex of the right pyriform sinus (*arrow*); some evidence of subtle infiltration or displacement of the paraglottic space fat is

present (*arrowhead*). **b** Axial image obtained during modified Valsalva maneuver. The right pyriform sinus expands somewhat less than the opposite one; the mucosal irregularity produced by the cancer is now better visible (*arrowheads*)

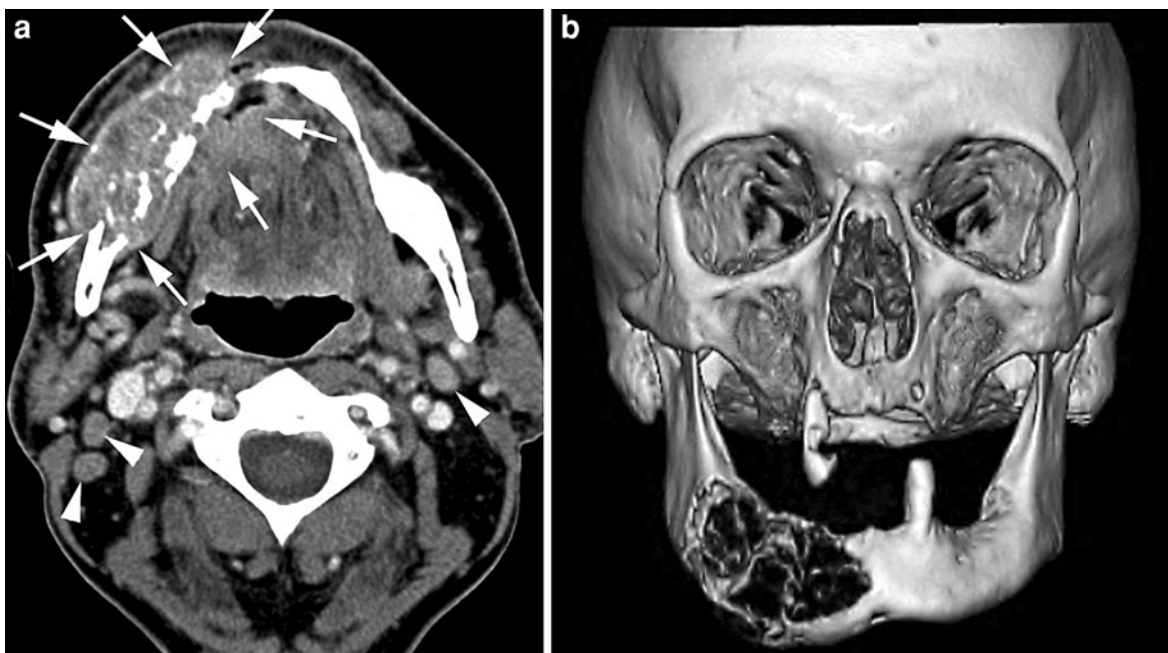


**Fig. 9 a** Axial contrast-enhanced MDCT-image. Large floor of the mouth cancer, massively invading the right side of the mandible (*arrows*). Several small but inhomogeneously

enhancing adenopathies are visible on both sides of the neck (*arrowheads*). **b** Extent of mandibular bone destruction can easily be appreciated on 3D reformatted

The use of parallel imaging grants the benefit of a reduced scan time with the same image quality, or a comparable scan time but with a better image quality. In practice this means that patient movement artifacts can be reduced and signal-to-noise ratio increased, making parallel imaging an ideal addition to head and neck MR imaging. However, as successful application of the parallel imaging reconstruction algorithm is very dependent on both magnetic field and receiver coil homogeneity, a combined use of several head and neck coils (see above) limits the use of parallel imaging. When using the newer systems with a large number of homogeneous receiver coils, application of parallel imaging is encouraged for comprehensive evaluation of the head and neck area.

Example parameters for head and neck MRI are listed in Table 3.

#### 4.2.4 Contrast Agents

In MR-studies for head and neck neoplasms, obtaining sequences before and after injection of gadolinium-DTPA (at a dose of 0.1–0.2 mmol/kg body weight) is mandatory. Most neoplasms will show increased signal intensity after contrast-agent injection. This will usually increase the contrast between the tumor and the surrounding lesions. However, tumors infiltrating bone marrow may become less well visible after contrast injection, as their signal intensity may become similar to that of the surrounding bone marrow; this problem can be solved by obtaining a fat-suppressed sequence

**Table 3** Example parameters for full head and neck examination at **a** 1.5T with combination of head and neck coils and at **b** 3T with integrated head and neck coil

Parameter	Pre-contrast T2-weighted imaging	Pre-contrast diffusion-weighted imaging	Dynamic contrast-enhanced imaging	Pre- and Post-contrast T1-weighted imaging
<i>(A) 1.5T</i>				
Sequence type	T2-weighted Turbo spin-echo (TSE)	Spin-echo echoplanar imaging (SE-EPI)	3D spoiled gradient echo	T1-weighted Turbo spin-echo (TSE)
Field of view (mm)	203 × 250	203 × 250	225 × 300	203 × 250
Matrix	291 × 512	104 × 128	134 × 256	333 × 512
Pixel size (mm)	0.70 × 0.49	1.95 × 1.95	1.68 × 1.17	0.61 × 0.5
Number of slices	48	48	48	30
Slice thickness (mm)	4	4	4.4	4
Interslice gap (mm)	0.4	0.4	0	0
TR/TE (ms)	3,080/106	7,400/84	4.3/1.6	532/8.3
Phase encoding direction	Anteroposterior	Anteroposterior	Anteroposterior	Anteroposterior
Averages	2	3	1	2
Phase partial Fourier	0.875	0.75	0.75	1
Bandwidth (Hz/pixel)	136	1,502	350	195
Turbo factor/echo-train length ( )	19	104	–	7
Parallel imaging factor	–	–	–	–
B-values (s/mm <sup>2</sup> )	–	0, 50, 100, 500, 750, 1,000	–	–
Saturation	–	Fatsat	–	- (If needed)
Scan time (min:sec)	5:42	6:03	3:29 for 25 measurements	5:11

(continued)

**Table 3** continued

Parameter	Pre-contrast T2-weighted imaging	Pre-contrast diffusion-weighted imaging	Dynamic contrast-enhanced imaging	Pre- and Post-contrast T1-weighted imaging
<i>(B) 3T</i>				
Sequence type	T2-weighted Turbo spin-echo (TSE)	Spin-echo echoplanar imaging (SE-EPI)	3D spoiled gradient echo	T1-weighted Turbo spin-echo (TSE)
Field of view (cm)	240 × 220	228 × 190	294 × 395	240 × 220
Matrix	377 × 440	116 × 100	248 × 360	303 × 400
Pixel size (mm)	0.64 × 0.50	1.96 × 1.90	1.19 × 1.10	0.79 × 0.55
Number of slices	54	2 stacks of 28	162	55
Slice thickness (mm)	3.5	4	1.3	3.5
Interslice gap (mm)	0.4	0.4	0	0.35
TR/TE (ms)	4,476/90	5,045/64	3.4/1.65	666/16
Phase encoding direction	Anteroposterior	Anteroposterior	Anteroposterior	Anteroposterior
Averages	2	2	1	2
Phase partial Fourier	1	0.689	0.625	1
Bandwidth (Hz/pixel)	194	2,896	1,206	196
Turbo factor/echo-train length ()	24	61	–	7
Parallel imaging factor	2	2	2	3
B-values (s/mm <sup>2</sup> )	–	0, 50, 100, 500, 750, 1,000	–	–
Saturation	–	Short tau inversion recovery (STIR)	Spectral selection attenuated inversion recovery (SPAIR)	- (If needed)
Scan time (min:sec)	3:48	2 × 2:47	3:15 for 20 measurements	3:39

(see above). Tumor necrosis becomes better visible after injection of gadolinium; this is of particular importance in staging the neck nodes (see “[Neck Nodal Disease](#)”).

Ultra-small superparamagnetic iron oxide (USPIO) particles are captured by macrophages in normally functioning lymph nodes. As a result, signal intensity reduction is observed in tissues accumulating these particles because of the susceptibility effects of iron oxide. Metastatic lymph nodes show a hyperintensity on sequences weighted to these effects. Some promising results have been

obtained in the head and neck, but technical problems regarding motion, susceptibility artifacts and spatial resolution still need to be solved (Sigal et al. 2002).

#### 4.2.5 Additional MRI Techniques

Although defining the extent of the primary tumor is often possible based on anatomical criteria, identification of small nodal metastasis remains challenging. Also the distinction of post-therapeutic tissue changes from residual tumor may be difficult. In recent years, progress has been made in the application

of functional MRI in head and neck imaging (Vandecaveye et al. 2010).

While the clinical application of MR-spectroscopy (MRS) remains challenging, dynamic contrast-enhanced MRI (DCE-MRI) and diffusion-weighted MRI (DWI) can now be used as complementary imaging tools in the locoregional imaging evaluation of head and neck cancer.

#### 4.2.5.1 Dynamic Contrast-Enhanced Magnetic Resonance Imaging

The tumoral vascular network is substantially different from a morphological and functional point of view compared to normal blood vessels, resulting in a heterogeneous blood flow, with increased capillary permeability (Carmeliet and Jain 2000).

DCE-MRI uses serial imaging with high temporal resolution over a lesion or anatomical area prior to, during and after the bolus injection of a gadolinium-based contrast agent to depict the perfusion properties of tumoral lesions. For head and neck imaging, a T1-weighted gradient-echo sequence is usually preferred over T2\*-based dynamic susceptibility contrast MRI (DSC-MRI). Compared with DSC-MRI, DCE-MRI requires less contrast agent and is far less prone to susceptibility artifacts. Most importantly, the signal intensity changes caused by the contrast agent are much slower than in DSC-MRI, and therefore a lower time resolution is allowed (around 4–8 s/volume), providing the opportunity to obtain larger anatomical coverage and higher spatial resolution images, while retaining perfusion information (Fig. 10). Also, the positive contrast enhancement used in the T1-weighted DCE-MRI allows more easy lesion identification compared to the negative contrast-enhancement of the T2\*-weighted DSC-MRI.

In both normal and tumoral tissue, the injected contrast will leak from the vessels into the interstitial space with a variable rate and will start to wash out when the interstitial concentration exceeds the intravascular concentration. The main parameters influencing this rate of interstitial contrast leakage are contrast inflow into the tissue, vessel wall permeability and the total vessel surface area (Padhani 2003).

The signal intensity curve, obtained from the consecutive sequences over time, holds information about tumor perfusion, tracer uptake and blood

volume. After the contrast injection, the enhancement pattern will typically consist of three phases: the upslope or rapid arterial enhancement, the point of maximum enhancement and delayed washout. The dynamic signal enhancement on T1-weighted DCE-MRI can be assessed by semi-quantitative evaluation of the signal intensity curve or by quantification of the change of contrast-agent concentration using pharmacokinetic modeling techniques. Semi-quantitative parameters evaluate discrete points of the signal intensity curve while ignoring the information in the rest of the curve; these include the maximal contrast-enhancement, time to maximal contrast-enhancement (time to peak) and the speed of arterial contrast-enhancement (initial slope) (Fig. 10). Their main advantage is their robustness, facilitating their use in clinical routine, although it should be kept in mind that semi-quantitative parameters do not reflect contrast medium concentration in tissues and may show variability because of scanner settings and differences in interpatient cardiovascular physiology (Padhani 2003). Therefore, in order to decrease intra- and interpatient variability during treatment follow-up, normalization of contrast-uptake may be done by analyzing contrast-enhancement in a feeding artery and normalizing the tissue measurements to this arterial input function (AIF) (Port et al. 2001).

For quantitative analysis, the entire contrast-time-curve is fitted by a curve model based on biological assumptions, such as blood volume, blood flow or permeability. Quantitative parameters that are investigated include the volume transfer constant of the contrast agent ( $K^{\text{trans}}$ ) and the rate constant ( $k_{\text{ep}}$ ), which are calculated based on a two compartment model correlating the tissue tracer concentration to the difference between arterial plasma and interstitial fluid concentrations (Tofts and Kermod 1991). These parameters have the advantage that they show closer correlation to underlying biologic processes of the vasculature, such as the permeability surface area and flow. However, quantified models are more complex to analyze, less robust and more susceptible to artifacting, making them more difficult to use in clinical routine.

An intermediate solution to quantify perfusion is the use of the initial area under the signal intensity curve (IAUC) or contrast medium concentration curve (IAUGC) (Padhani 2003).

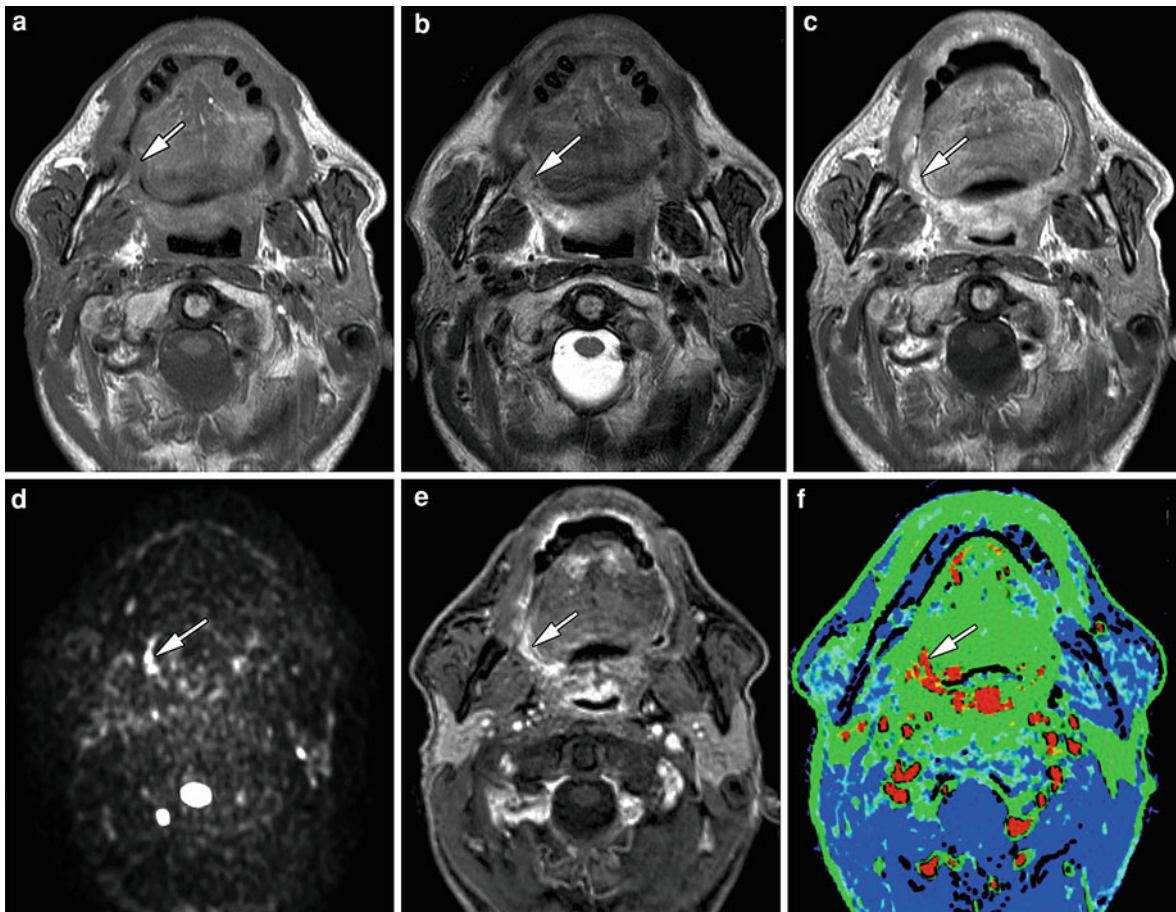


**Fig. 10** Patient with persistent pain in the right oropharyngeal area, 4 months after end of chemoradiotherapy for a base of tongue cancer. T1-weighted (a), T2-weighted (b) and contrast-enhanced T1-weighted spin-echo sequence (c) show some soft tissue thickening in the right glossotonsillar sulcus and anterior tonsillar pillar (arrow). B1000 diffusion-weighted weighted

image (d) shows hyperintensity in this area, while the native dynamic contrast-enhanced image (e) and corresponding perfusion map (*initial slope*, f) indicate hypervascularity (arrows). These findings are suspect for persistent or recurrent tumor. Histopathology after surgical resection confirmed presence of squamous cell carcinoma

#### 4.2.5.2 Diffusion-Weighted Magnetic Resonance Imaging

DWI allows for tissue characterization based on changes in the random movement of tissue water molecules (Le Bihan et al. 1988). In solid malignant tumors, the high cellular density, intact cellular membranes and diminished extravascular extracellular space (EES), restricts the random movement of water (Fig. 10). Contrary, in necrosis and inflammation, the low cellular density and increased EES facilitates the random water movement.

Spin-echo EPI-based DWI (SE-EPI-DWI) is most frequently used for imaging of head and neck cancer. The major advantage of an EPI readout sequence is

the inherent rapidity as it is a single-shot sequence without the need for refocusing radiofrequency pulses. This allows to scan relatively large volumes with multiple b-values in a short time period, making the technique suitable for the simultaneous evaluation of the primary tumor site and all nodal stations in the head and neck (Vandecaveye et al. 2010). As a drawback, SE-EPI-DWI is highly sensitive to susceptibility artifacts, possibly reducing diagnostic quality. Single-shot turbo spin-echo (SS-TSE)-DWI may be considered as an alternative sequence for EPI-DWI, as this sequence lacks these kinds of artifacts (De Foer et al. 2008). However, because of the inherent need of  $180^\circ$  spin-echo pulses, SS-TSE-DWI

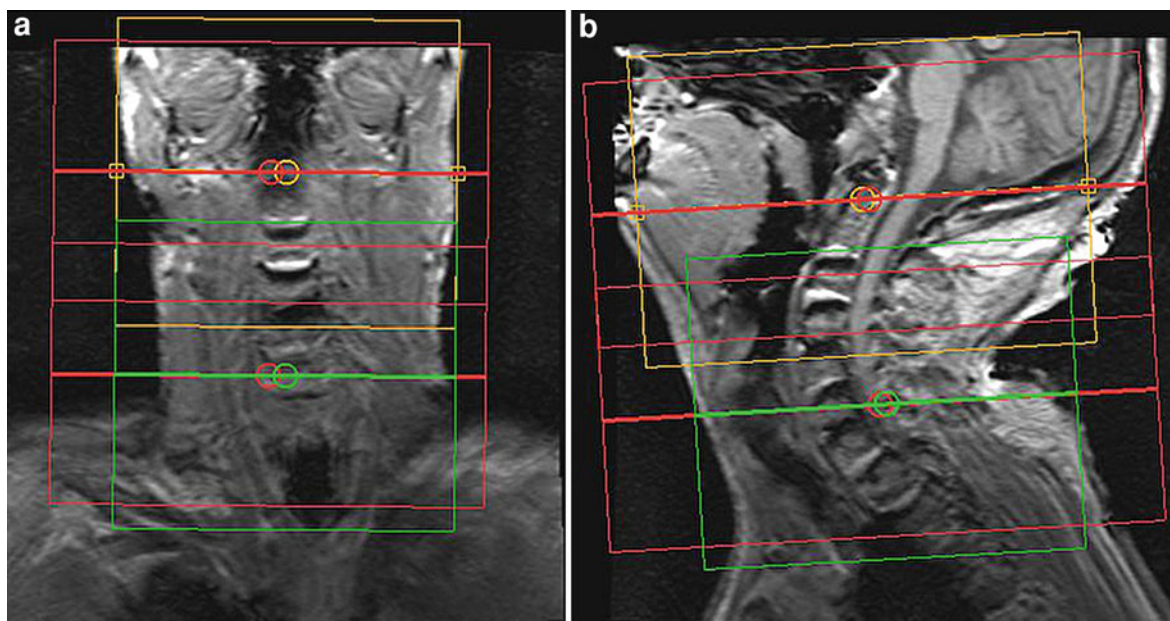


**Fig. 11** Localizer image in the coronal (a) and sagittal plane (b), obtained on a 3T system. The imaging volumes (red boxes) are divided into two sub-volumes, respectively extending from the skull base to the level of the hyoid and from the hyoid to the

thoracic inlet. Shim boxes (green box and orange box) have been adapted in the phase encoding direction, excluding the air around the head and neck

is limited by a high specific absorption rate (SAR), and is time consuming; therefore it cannot be used for screening of the entire neck or for examinations that require the inclusion of multiple b-values. Additionally, the higher echo time (TE) of SS-TSE-DWI compared to SE-EPI-DWI leads to an unfavorable SNR making the detection of tumoral lesions more difficult. Therefore, SS-TSE-DWI is only useful for evaluation of a limited anatomical area, where susceptibility artifacts make the application of SE-EPI-DWI nearly impossible.

Because of the sensitivity of DWI to artifacts, a number of technical optimizations are pivotal to preserve diagnostic imaging quality. First, it is important that the shortest possible TE is selected, maximizing the signal-to-noise ratio, and minimizing susceptibility and fat-shift artifacts. This requires the scanner to be equipped by a strong gradient system and the use of a high bandwidth. Second, one should rather not use unrealistically high DW imaging matrices, as this increases the echo-train length, introducing T2\* and susceptibility artifacts. In most clinical settings, an imaging matrix of 128 is sufficient, although in low-susceptibility areas it can be increased up to 192. The third and most important

issue concerns positioning of the shim block, which should be placed manually instead of using the automatic shim leading to a strong decrease of distortion artifacts (Fig. 11). Currently, no uniform guidelines exist to optimize shimming, but usually, the shim should be tailored around the total head and neck, excluding large areas of air surrounding the neck at 3T MR-systems. At 1.5T MR-systems, or when using a combination of a standard head coil and 2-channel dedicated surface coil, the shim box should only cover the spine and deep muscles of the neck, while excluding as much as possible any moving or air-containing structures.

Finally, when DWI needs to cover the entire head and neck, the imaging volume can be subdivided into two separate but spatially linked scan volumes; one extending from the skull base down to the level of the hyoid, and the second one extending further down to the aortic arch. This allows closer positioning of each imaging stack to the isocenter of the magnet, minimizing geometric distortion and failed fat suppression at the slices further away from the isocenter.

DWI can be evaluated in a qualitative and quantitative way. Qualitative analysis using DWI at a single high b-value (usually  $b = 1000 \text{ s/mm}^2$ ) offers

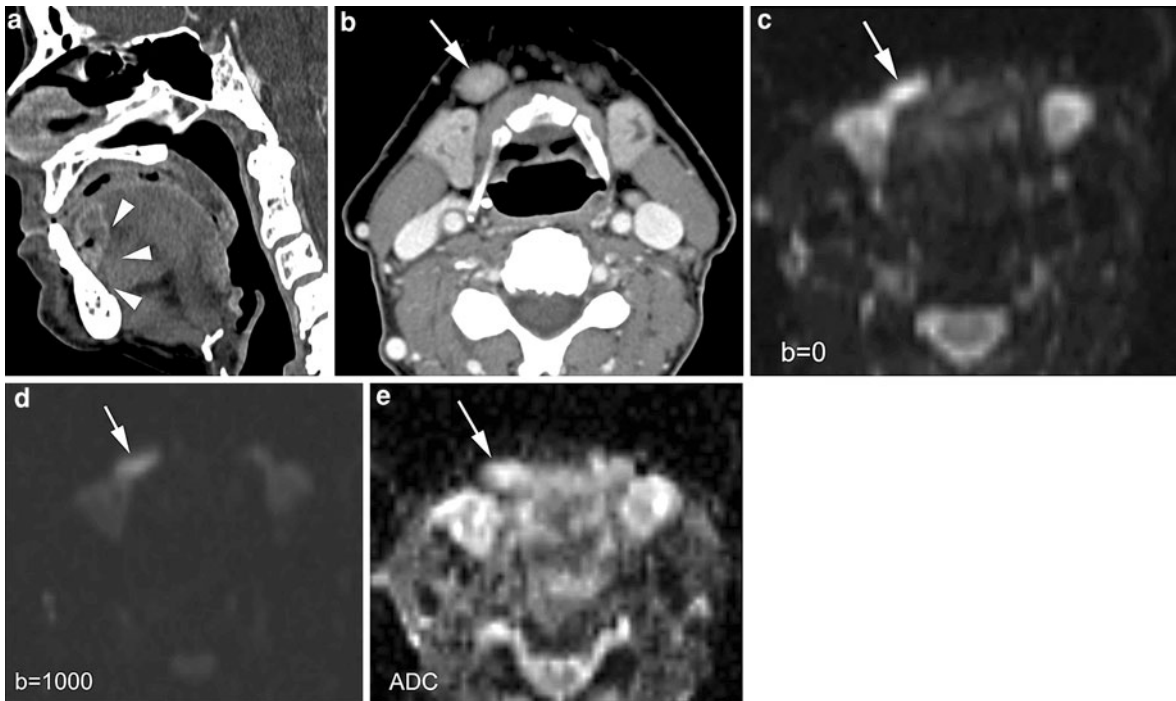


**Fig. 12** Patient suffering floor of the mouth cancer. **a** Sagittal contrast-enhanced MDCT-image shows primary tumor at the junction of the floor of the mouth and oral tongue (*arrowheads*). **b** Axial MDCT-image. Slightly enlarged lymph node (minimal axial diameter 12 mm) in the submandibular region (*arrow*): suspect for metastatic adenopathy. **c–e** Axial diffusion-weighted MR-images. Compared to the  $b = 0$  image

(**c**), the signal clearly reduced in the adenopathy (*arrow*) on the  $b = 1000$  image (**d**), indicating easy diffusion of water protons. The ADC-map (**e**) shows a relative high signal ( $ADC > 0.00130 \text{ mm}^2/\text{s}$ ). These findings are consistent with a benign adenopathy. After neck dissection, histologically no tumor was found in this lymph node

high sensitivity for detection of tumoral disease but has relatively low specificity (Takahara et al. 2004). Such images can be used for the rapid depiction of potentially tumoral localizations. However, DWI-based tissue characterization, especially of lymph nodes, often requires additional calculation of the apparent diffusion coefficient (ADC) (Fig. 12).

In head and neck DWI, 3 up to 6 b-values ranging from 0 to  $1000 \text{ s/mm}^2$  are preferentially used. The large number of b-values improves the accuracy of the ADC-calculation, by minimizing the influence of movement and noise propagation. Also, in highly vascular tumors, the addition of non-zero low b-values can be used to eliminate vascular contributions that may falsely increase ADC values by an additional but variable influence of microperfusion (Thoeny et al. 2005). A DWI-sequence with six b-values and 4 mm slice thickness typically takes around 5 min on a 1.5 Tesla system, and around 3 min on a 3 Tesla system.

## 5 Nuclear Imaging

### 5.1 Physical Aspects

Positron emission tomography (PET) allows evaluation of the biodistribution of small amounts of positron-emitting radiopharmaceuticals and is considered the most sensitive and specific technique for in vivo imaging of metabolic pathways and receptor–ligand interactions in the tissues of men (Jones 1996). PET uses radioisotopes of natural elements, such as oxygen-15, carbon-11, nitrogen-13 and fluorine-18, which can be used for labeling of most biomolecules, without altering their biochemical properties.

Positron-emitting isotopes decay by emission of a positron, which is the positively charged antiparticle of the electron. Positrons are formed during the decay of nuclides that have a large number of protons in their nuclei compared with the number of neutrons,

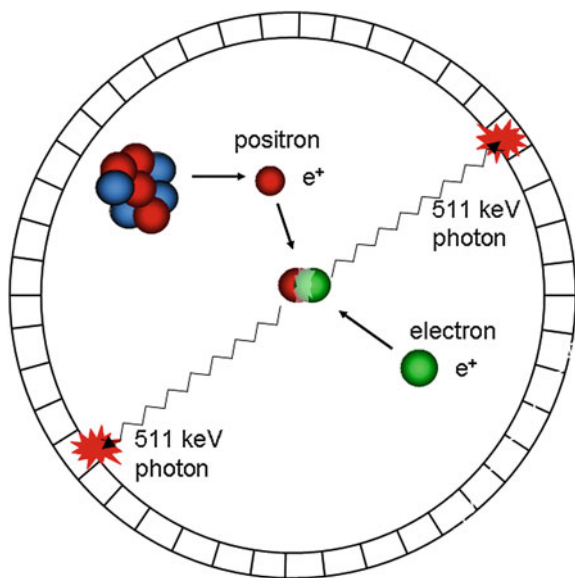


**Fig. 13** After the decay of a positron-emitting radioisotope, the positron annihilates with an electron, resulting in the creation of two annihilation photons, each having an energy of 511 keV. In a PET camera, a large number of detectors are installed in a ring-shaped pattern around the patient, enabling the simultaneous detection of the opposed photons within a narrow time-window, the so-called “coincidence detection”

which makes them unstable. After its emission, the positron travels a short distance until it annihilates with an electron. In this process, the positron and electron masses are converted into 2 photons that travel apart in nearly opposite directions (180°) with an energy of 511 keV each (Fig. 13). PET tomographs are designed to detect these photon pairs and to reconstruct tomographic images of the regional tracer distribution. Detector pairs are installed in a ring-shaped pattern for the detection of the opposed photons within a narrow time-window, enabling the so-called “coincidence detection”. Because of this “electronic” collimation, PET does not require collimators as they are necessary in single photon measurements with gamma cameras. This results in a significantly higher sensitivity of PET compared to SPECT. The sensitivity of PET can be further improved by adding extra detector rings, increasing the axial coverage (Townsend 2008). Compared with SPECT, PET has a relatively high spatial resolution of 4–6 mm. Recent PET cameras are equipped with detectors of smaller size, enabling the detection of

smaller lesions which is particularly important in patients with head and neck cancer. However, the physics of PET impose certain well-known limitations on the spatial, temporal and contrast resolution that can be attained in a particular situation. Both the range the positron travels until annihilation and the residual momentum of the positron–electron pair degrade the spatial resolution and will limit the resolution of future whole body PET cameras to approximately 2 mm.

## 5.2 Radiopharmaceuticals

### 5.2.1 <sup>18</sup>Fluorodeoxyglucose

The tracer most commonly used worldwide is Fluorine-18-labeled 2-fluoro-2-deoxy-D-glucose, [<sup>18</sup>F]FDG. This is a D-glucose molecule in which a hydroxyl group in the 2-position is replaced by a positron-emitting <sup>18</sup>F. Several decades ago, Warburg et al. described the higher rate of glucose metabolism in cancer cells compared to non-malignant tissue (Warburg 1956). After malignant transformation, there is an increased expression of epithelial glucose transporter proteins and an up-regulation of hexokinase activity. After intravenous injection, FDG distributes throughout the body in proportion to glucose metabolism of tissues. Glucose transporters facilitate FDG uptake in tumor cells and hexokinase subsequently phosphorylates FDG to FDG-6-phosphate. FDG-6-phosphate is not metabolized in the glycolytic pathway because it lacks a hydroxyl group in position-2. As most tumor cells do not contain significant amounts of glucose-6-phosphatase, FDG-6-phosphate will accumulate in the cell, resulting in the so-called “metabolic trapping” (Fig. 14) (Pauwels et al. 1998).

It has been demonstrated that increased FDG uptake by malignant cells, although a function of the proliferative activity, is mainly related to the number of viable tumor cells (Higashi et al. 1993). However, some benign tumors can also consume considerable amounts of glucose, as can be seen in Warthin tumors of the parotid gland. In addition, inflammatory tissue may exhibit an increased FDG uptake due to glycolytic activity in neutrophils, eosinophils, macrophages and proliferating fibroblasts, to a degree sometimes more marked than in malignant cells, resulting in a false positive FDG-signal (Kubota et al. 1992). This can be a problem in the field of therapy monitoring, where posttreatment inflammation may raise the overall FDG uptake, causing an

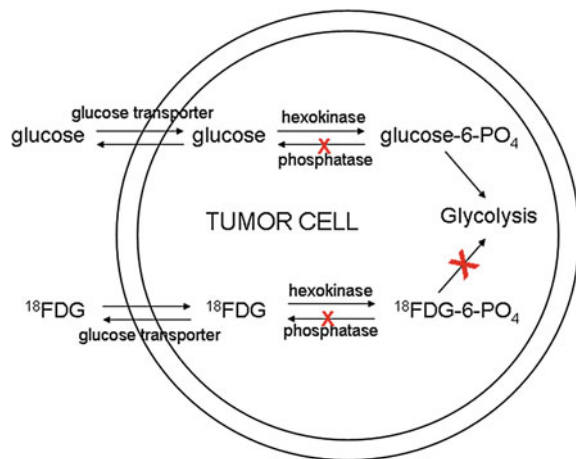


**Fig. 14** Uptake kinetics of glucose and FDG in a tumor cell. Glucose transporters facilitate FDG uptake in tumor cells and hexokinase subsequently phosphorylates FDG. The phosphorylated product FDG-6-phosphate is not metabolized in the glycolytic pathway and the activity of glucose-6-phosphatase in tumor tissue is low, resulting in the metabolic trapping of FDG-6-phosphate in the tumor cell

underestimation of treatment effectivity and a decrease in the specificity of FDG-PET (Schöder et al. 2009). For this reason FDG-PET after radiotherapy should not be performed before 8–12 weeks after the end of treatment of head and neck tumors. Alternatively, some more tumor-specific tracers have been proposed, which should be less sensitive to inflammatory conditions.

### 5.2.2 $^{18}\text{F}$ Fluorothymidine

$^{18}\text{F}$ -labeled fluorothymidine,  $^{18}\text{F}$ FLT, is utilized in oncology as a marker of cellular proliferation. Thymidine is a native nucleoside, which is used by cells for DNA replication. FLT enters the cell, undergoes phosphorylation by thymidine kinase 1 and is being accumulated in the cytosol instead of being trapped into DNA. Thymidine kinase 1 activity is high in proliferating cells and low in quiescent cells.

### 5.2.3 $^{18}\text{F}$ FET and $^{11}\text{C}$ -MET

Labeled amino acid analogs like  $^{18}\text{F}$ -fluoro-ethyl-tyrosine ( $^{18}\text{F}$ FET) and  $^{11}\text{C}$ -methionine ( $^{11}\text{C}$ -MET) have been developed for tumor detection. Increased amino acid metabolism results in an accumulation of amino acids in tumor cells. Compared to FDG, the uptake of amino acids in inflammatory cells is lower.

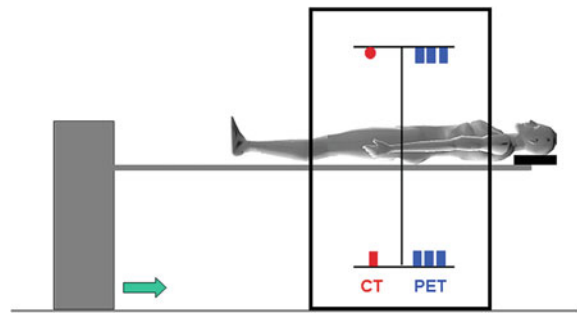


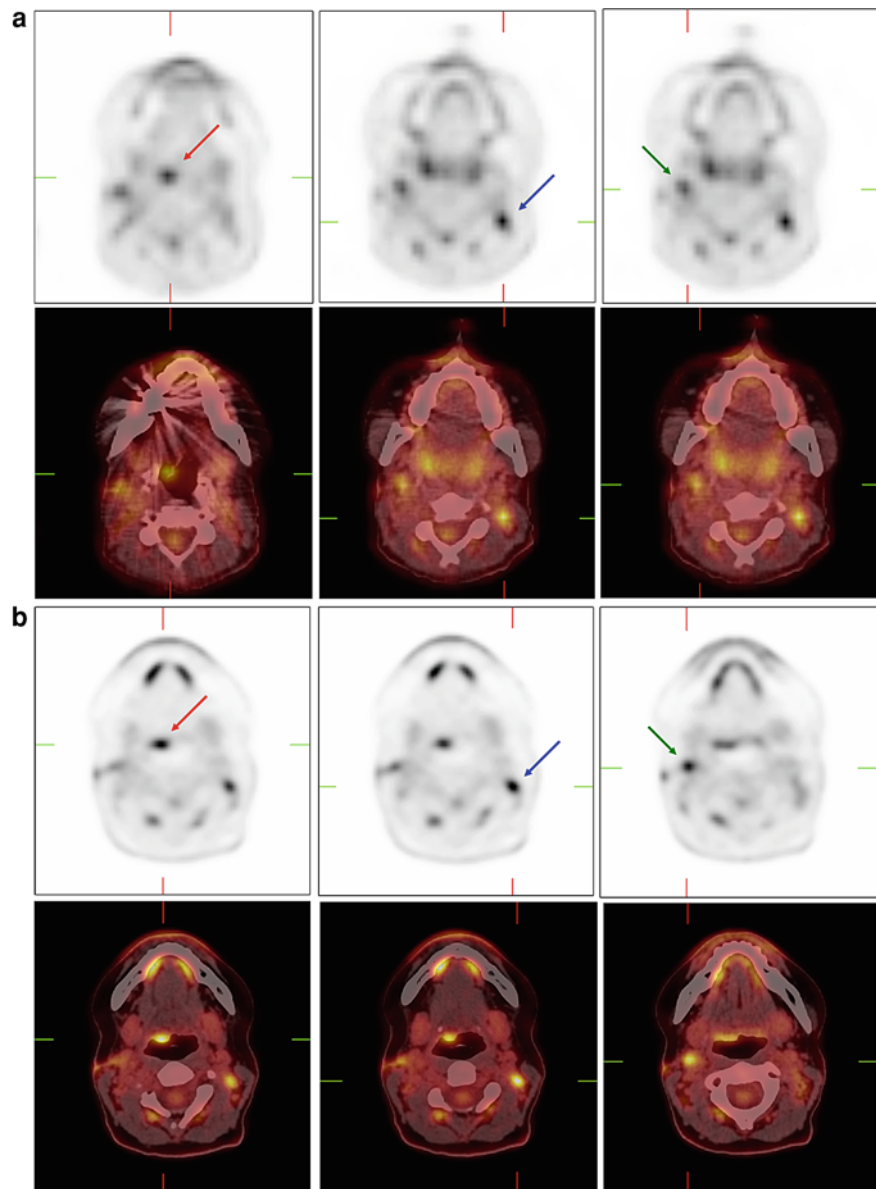
**Fig. 15** A schematic design of a modern PET/CT camera, combining a PET camera and a diagnostic CT-scanner within one gantry. A standard whole body FDG-PET/CT protocol is started 60 min after the intravenous injection of FDG and includes a low-dose spiral CT acquisition without contrast, followed by a PET acquisition of the same region and followed by a complementary contrast-enhanced CT-study

## 5.3 Technical Aspects of FDG-PET and Integrated FDG-PET/CT in Head and Neck Cancer

FDG-PET relies on the detection of metabolic alterations in cancer cells, independent of structural features as provided by morphologic imaging techniques like contrast-enhanced CT and MRI. Especially in the post-treatment setting, morphologic imaging modalities have distinct limitations in accurate identification of viable tumor within residual masses, in the identification of small tumor deposits (e.g. in normal-size lymph nodes), and in the characterization of secondary enlarged inflammatory lymph nodes (McCabe and Rubinstein 2005). Postradiation changes and anatomic distortions limit the diagnostic accuracy of these anatomic-based imaging studies in the head and neck region. Since biochemical and cellular changes precede size reduction, there is an increasing interest in response imaging in-vivo using molecular imaging with FDG-PET. Moreover, FDG-PET has an advantage over conventional imaging because of its whole body coverage and its sensitivity to distant lesions that may be missed by conventional imaging.

A major limitation of FDG-PET in the neck is the inadequate anatomic information inherent in metabolic imaging. The interpretation of FDG-PET images of the head and neck is particularly difficult because of the presence of multiple sites showing a variable degree of physiological FDG accumulation, such as the salivary glands, lymphoid tissues, muscles and

**Fig. 16** FDG-PET and fused FDG-PET/CT slices illustrating the improvement in image quality between standard whole body images and dedicated high-resolution head and neck images in a patient with a lymph node positive for squamous cell carcinoma on the right side of the neck, and an unknown primary tumor. **a** Whole body images demonstrate avid FDG uptake at the base of the tongue (*red arrow*) and at both sides of the neck (*blue and green arrows*). Interpretation of these FDG spots is difficult because of CT-related artifacts, insufficient image resolution of both PET and CT, and the presence of FDG uptake in brown fat and muscle. **b** Dedicated head and neck images clearly show the primary tumor at the base of the tongue (*red arrow*) and a positive lymph node at both sides of the neck (*blue and green arrows*). These dedicated fused head and neck images allow easy differentiation between tumor and physiological FDG uptake in brown fat or muscle



brown adipose tissue (“USA-Fat”). The introduction of combined PET/CT scanners has overcome this problem by providing coregistered metabolic and anatomic information (Fig. 15). Combined PET/CT has proven to be more accurate than stand-alone FDG-PET by improving the differentiation between physiologic and pathologic FDG uptake and by providing a more accurate tumor localization, hence reducing the number of equivocal findings (Goshen et al. 2006). In addition, FDG-PET image quality can be improved by instructing patients not to speak

during the FDG uptake phase and by pharmacological interventions with diazepam, reducing muscular uptake, or with propranolol, reducing FDG uptake in brown adipose tissue.

Until today, independent of the tumor type, clinically combined PET/CT imaging is usually performed as a whole body imaging tool, which has intrinsic limitations in terms of resolution (affecting sensitivity) and false positive findings (affecting specificity). Moreover, the CT-part of this examination is most often performed as a low-dose non-diagnostic non-contrast CT, which is

sufficient for attenuation correction and anatomic correlation of the PET images, but does not offer the image quality of a diagnostic CT-scan. Hence, this whole body approach using general reconstruction algorithms is less suitable for imaging of a complex and dense anatomic region like the neck. Recent data advocate the use of high-resolution head and neck PET/CT protocols for the detection of small lymph node metastases in the neck (Vogel et al. 2005; Rodrigues et al. 2009). In such a setting, whole body imaging is being performed for the detection of metastatic disease, while dedicated high-resolution head and neck PET/CT imaging is added for the detection of the primary tumor and/or lymph node metastases in the neck. Ideally, dedicated head and neck PET/CT imaging is being performed with the arms down (along the side of the patient) and should include a diagnostic CT-scan with the use of intravenous contrast. The PET acquisition and reconstruction parameters should be optimized for the head and neck region and smaller pixels should be used, reducing the partial volume effect which causes an underestimation of FDG activity in all lesions smaller than twice the spatial resolution. These improvements enable to optimize integrated FDG-PET/CT imaging for the detection of small primary tumors and small nodal metastases in the head and neck region (Fig. 16).

Because of further technical improvements and the introduction of newer, more specific radiopharmaceuticals, the role of PET/CT imaging in the management of head and neck tumors is likely to become even more important in the future.

## References

- Carmeliet P, Jain RK (2000) Angiogenesis in cancer and other diseases. *Nature* 407:249–257
- Curtin HD, Ishwaran H, Mancuso AA et al (1998) Comparison of CT and MR imaging in staging of neck metastases. *Radiology* 207:123–130
- De Foer B, Vercruyse JP, Bernaerts A et al (2008) Detection of postoperative residual cholesteatoma with non-echo-planar diffusion-weighted magnetic resonance imaging. *Otol Neurotol* 29:513–517
- Goshen E, Davidson T, Yahalom R et al (2006) PET/CT in the evaluation of patients with squamous cell cancer of the head and neck. *Int J Oral Maxillofac Surg* 35:332–336
- Henrot P, Blum A, Toussaint B, Troufleau P, Stines J, Roland J (2003) Dynamic maneuvers in local staging of head and neck malignancies with current imaging techniques: principles and clinical applications. *Radiographics* 23:1201–1213
- Higashi K, Clavo AC, Wahl RL (1993) In vitro assessment of 2-fluoro-2-deoxy-D-glucose, L-methionine and thymidine as agents to monitor the early response of a human adenocarcinoma cell line to radiotherapy. *J Nucl Med* 34:773–779
- Jones T (1996) The imaging science of positron emission tomography. *Eur J Nucl Med* 23:807–813
- Keberle M, Tschammler A, Hahn D (2002) Single-bolus technique for spiral CT of laryngopharyngeal squamous cell carcinoma: comparison of different contrast material volumes, flow rates, and start delays. *Radiology* 224:171–176
- Kubota R, Yamada S, Kubota K et al (1992) Intratumoural distribution of fluorine-18-fluorodeoxyglucose in vivo: high accumulation in macrophages and granulation tissues studied by microautoradiography. *J Nucl Med* 33:1972–1980
- Le Bihan D, Breton E, Lallemand D, Aubin ML, Vignaud J, Laval-Jeantet M (1988) Separation of diffusion and perfusion in intravoxel incoherent motion MR imaging. *Radiology* 168:497–505
- Lell MM, Greess H, Hothorn T, Janka R, Bautz WA, Baum U (2004) Multiplanar functional imaging of the larynx and hypopharynx with multislice spiral CT. *Eur Radiol* 14:2198–2205
- Magnano M, Bongioannini G, Cirillo S et al (2005) Virtual endoscopy of laryngeal carcinoma: is it useful? *Otolaryngol Head Neck Surg* 13:776–782
- McCabe KJ, Rubinstein D (2005) Advances in head and neck imaging. *Otolaryngol Clin North Am* 38:307–319 vii
- Padhani AR (2003) MRI for assessing antivasular cancer treatments. *Br J Radiol* 76:S60–S80
- Pauwels E, McCready VR, Stoot JH et al (1998) The mechanism of accumulation of tumour-localising radiopharmaceuticals. *Eur J Nucl Med* 25:277–305
- Port RE, Knopp MV, Brix G (2001) Dynamic contrast-enhanced MRI using Gd-DTPA: interindividual variability of the arterial input function and consequences for the assessment of kinetics in tumors. *Magn Reson Med* 45:1030–1038
- Robert YH, Chevalier D, Rocourt NL et al (1993) Dynamic maneuver acquired with spiral CT in laryngeal disease. *Radiology* 189:298–299
- Rodrigues RS, Bozza FA, Christian PE et al (2009) Comparison of whole-body PET/CT, dedicated high-resolution head and neck PET/CT, and contrast-enhanced CT in preoperative staging of clinically M0 squamous cell carcinoma of the head and neck. *J Nucl Med* 50:1205–1213
- Schöder H, Fury M, Lee N, Kraus D (2009) PET monitoring of therapy response in head and neck squamous cell carcinoma. *J Nucl Med* 50 Suppl 1:74S–88S
- Sigal R, Vogl T, Casselman J et al (2002) Lymph node metastases from head and neck squamous cell carcinoma: MR imaging with ultrasmall superparamagnetic iron oxide particles (Sinerem MR)—results of a phase-III multicenter clinical trial. *Eur Radiol* 12:1104–1113
- Silverman PM, Zeiberg AS, Sessions RB, Troost TR, Zeman RK (1995) Three-dimensional imaging of the hypopharynx and larynx by means of helical (spiral) computed tomography. Comparison of radiological and otolaryngological evaluation. *Ann Otol Rhinol Laryngol* 104:425–431
- Takahara T, Imai Y, Yamashita T, Yasuda S, Nasu S, Van Cauteren M (2004) Diffusion weighted whole body imaging with background body signal suppression (DWIBS):

- technical improvement using free breathing, STIR and high resolution 3D display. *Radiat Med* 22:275–282
- Takes RP, Knecht P, Manni JJ et al (1996) Regional metastasis in head and neck squamous cell carcinoma: revised value of US with US-guided FNAB. *Radiology* 198:819–823
- Takes RP, Righi P, Meeuwis CA et al (1998) The value of ultrasound with ultrasound-guided fine-needle aspiration biopsy compared to computed tomography in the detection of regional metastases in the clinically negative neck. *Int J Radiat Oncol Biol Phys* 40:1027–1032
- Thoeny HC, De Keyzer F, Vandecaveye V et al (2005) Effect of vascular targeting agent in rat tumor model: dynamic contrast-enhanced versus diffusion-weighted MR imaging. *Radiology* 237:492–499
- Tofts PS, Kermode AG (1991) Measurement of the blood-brain barrier permeability and leakage space using dynamic MR imaging. 1. Fundamental concepts. *Magn Reson Med* 17:357–367
- Townsend D (2008) Dual-modality imaging: combining anatomy, function. *J Nucl Med* 49:938–955
- van den Brekel MW, Castelijns JA, Stel HV et al (1991) Occult metastatic neck disease: detection with US and US-guided fine-needle aspiration cytology. *Radiology* 180:457–461
- Vandecaveye V, De Keyzer F, Dirix P et al (2010) Applications of diffusion-weighted magnetic resonance imaging in head and neck squamous cell carcinoma. *Neuroradiology* 52:773–784
- Vogel WV, Wensing BM, van Dalen JA et al (2005) Optimised PET reconstruction of the head and neck area: improved diagnostic accuracy. *Eur J Nucl Med Mol Imaging*. 32:1276–1282
- Warburg O (1956) On the origin of cancer cells. *Science* 123:309–314
- Wirth S, Meindl T, Treitl M, Pfeifer KJ, Reiser M (2006) Comparison of different patient positioning strategies to minimize shoulder girdle artifacts in head and neck CT. *Eur Radiol* 16:1757–1762